AIAA 97-0051

# Validation of Thermal Ice Protection Computer Codes: Part 3- The Validation of ANTICE

K. Al-Khalil, C. Horvath
Cox & Company, Inc., New York, NY
D. Miller
NASA Lewis Research Center, Cleveland, OH
W. Wright
NYMA, Inc., Brook Park, OH

35th Aerospace Sciences
Meeting & Exhibit
January 6-7, 1997 / Reno, NV

# VALIDATION OF NASA THERMAL ICE PROTECTION COMPUTER CODES PART 3 - THE VALIDATION OF ANTICE

Kamel M. Al-Khalil*, Charles Horvath**
Cox & Company, Inc.
200 Varick Street
New York, NY 10014

Dean R. Miller†
NASA Lewis Research Center
21000 Brookpark Road
Cleveland, OH 44135

William B. Wright‡
NYMA, Inc.
2001 Aerospace Parkway
Brookpark, OH 44142

## ABSTRACT

*An experimental program was generated by the Icing Technology Branch at NASA Lewis Research Center to validate two ice protection simulation codes: LEWICE/Thermal for transient electrothermal de-icing and anti-icing simulations, and ANTICE for steady state hot gas and electrothermal anti-icing simulations. An electrothermal ice protection system was designed and constructed integral to a 36 inch chord NACA0012 airfoil. The model was fully instrumented with thermocouples, RTD's, and heat flux gages. Tests were conducted at several icing environmental conditions during a two week period at the NASA Lewis Icing Research Tunnel. Experimental results of running-wet and evaporative cases were compared to the ANTICE* computer code predictions and are presented in this paper.

## Nomenclature

AOA = angle of attack of body with the freestream air (degrees)
$C_{pw}$ = specific heat (Btu/lbm.ºF)
h = heat transfer coefficient between the dry surface and the ambient air (Btu/hr.ft$^2$.ºF)
$h_f$ = film coefficient between the wet surface and the ambient air (Btu/hr.ft$^2$.ºF)
K = thermal conductivity (Btu/hr.ft.ºF)
LWC = liquid water content in the freestream (g/m$^3$)
Lv = water latent heat of vaporization (Btu/lbm)
MVD = mean volume droplet diameter in cloud (μm)
m = surface runback mass flow rate per unit span distance (lbm/ft.hr)
$m_{evap}$ = rate of surface water evaporation (lbm/hr.ft$^2$)
$m_{imp}$ = rate of water droplets impingement (lbm/hr.ft$^2$)
q = heater power density (W/in$^2$)
$q_{conv}$ = convective heat loss (W/in$^2$)
$q_{evap}$ = evaporative heat loss (W/in$^2$)
$q_{KE}$ = kinetic heat gain from droplets impact on surface (W/in$^2$)
$q_{sens}$ = sensible heat required to warm the impinging water droplets (W/in$^2$)
S = surface distance from stagnation, positive on the upper surface (in)
$T_{aw}$ = adiabatic wall temperature (ºF)
$T_s$ = skin temperature (ºF)
$T_{tot}$ = total ambient temperature (ºF)
T4 = static ambient temperature (ºF)
V = freestream velocity (mph)
β = droplets collection efficiency
ρ = mass density (lbm/ft$^3$)

*Engineering Scientist, Member AIAA
**De-icing Systems Engineer
†Aerospace Engineer, Member AIAA
‡Aerospace Engineer, Member AIAA

## I. Introduction

Extensive testing is normally required in the design of thermal ice protection systems. The cost involved can be somewhat prohibitive. Some designers reduce costs by relying upon computer simulations to get through the preliminary design stage. The total cost and development period involved can further be reduced if the simulation codes are proven and reliable. Additionally, the simulation codes may be utilized in the certification process, in conjunction with flight/tunnel testing, once approved by the FAA.

An experimental program was initiated and sponsored by the Icing Technology Branch at the NASA Lewis Research Center (LeRC) in an effort to validate two thermal ice protection simulation codes: LEWICE/Thermal simulates the transient response of electrothermal de-icing and anti-icing systems, and ANTICE simulates the steady state response of hot gas and electrothermal anti-icing systems. The effort was a partnership between NASA LeRC and five US industry members. Participants from industry assumed the role of technical advisors. Additionally, Cox & Company, Inc. provided the test article, test monitoring and control software/hardware, and engineering test support.

An overview of the program is discussed by Miller,[1] and the validation of the LEWICE/Thermal code is presented by Wright.[2] This particular paper is dedicated to the validation of the ANTICE code which is a two dimensional computer simulation of a composite structure with embedded heaters. It also simulates a hot gas anti-icing system. The code has a rivulet model to simulate the flow of runback water on the surface. Experimental anti-icing data will be presented, and comparison will be made to the ANTICE code predictions.

## II. Analytical Model

The computer code is based on an analytical thermodynamic model that was described in earlier studies by Al-Khalil.[3,4] The various modes of heat transfer occurring within an anti-iced aircraft surface and the collected water, referred to as “runback” when it flows on the surface, have been modeled. The mathematical formulation is based on 2-D steady-state heat transfer model along a surface streamline.

The temperature is assumed to vary in the streamwise direction and across the structure thickness (transverse direction). Spanwise variations are much smaller than those in the chordwise direction. The runback water flow is also assumed, as proven in several tunnel tests, to be in the streamwise direction on the aircraft surface.

The aircraft structure may be represented by a number of composite layers. Any single layer can be composed of several heater zones, each with a specified power density. The mathematical formulation of the energy balance equation in the structure is based on the control volume approach. The structure is subdivided into a number of grids in the streamwise and transverse directions. An equation is then written for each node in the discretized region using the laws of energy conservation (and mass conservation on the impinging supercooled water droplets).

Anti-icing of the aircraft surface may also be accomplished using a hot air system. This is currently modeled such that hot air of a given mass flowrate and an initial temperature is supplied to the inner surface in the vicinity of the stagnation line, and flows back into the cowl in the direction of surface streamlines. A user can also specify a distribution of variable heat flux at the surface to obtain an approximate system behavior as a first step in the design and/or analysis process (i.e., evaporative, running wet, or freezing runback).

Also modeled is the runback flow behavior on the surface: continuous surface coverage at the direct impingement regions, versus rivulet structure flow downstream. Rivulets are individual narrow streams of water. A stability analysis was performed for the prediction of rivulets.[3,4]

ANTICE requires the following information:

(1) Surface pressure coefficient distribution along a streamline.
(2) The distance between two adjacent surface streamlines representing a zone of interest in the analysis. This is an option for 3-D flows such as on swept wings or inlet nacelles.
(3) Collection efficiency distribution at the surface.

The above information may be obtained from flow and trajectory codes such as NASA’s LEWICE ice accretion code. In the current analytical predictions, LEWICE[5] v1.7 was used to obtain the latter information. Details on the numerical procedure are presented in Reference [4].

## III. Experimental setup

### III.1 Test Article

A NACA0012 airfoil, 6 ft span and 36" chord, was fitted with an electro-thermal ice protection system at the leading edge (LE) and mounted vertically in the NASA LeRC Icing Research Tunnel (IRT). The removable LE was 10" long, and the wooden afterbody was 26" long. The ice protection system consisted of seven heater bands, each 18 inches long in the spanwise direction, individually controlled by the Cox Thermal Test Management System (TTMS). For redundancy, a spanwise image mirror of the seven heaters was constructed around the center line of the airfoil. The total heated spanwise length was 3 ft, and the total heated wrap distance in the chordwise direction was 7.75 inches.

A guard heater (8" span x 12" wrap) was installed on each end of the heated area along the airfoil span. The guard heaters were used to maintain as much of the airfoil clean of ice to prevent flow disturbances from affecting the measurement locations near the centerline. The total number of heated channels was 18.

Figure 1 shows a cross-section of the LE where zone A is 0.75" wide, zones B, C, D, and E are 1" wide, and finally zone F and G are 1.5" wide. Zones B, D, and F are on the IRT control room side. During the manufacturing process, the heater lay-up was accidentally shifted towards zones C, D, and G. The shift was estimated at about 0.19" during the tunnel tests when different amounts of surface runback were observed on each side of the airfoil. This heater shift was modeled in the computer code for a proper comparison between the experimental data and the analytical predictions.

Figure 2 illustrates the material composition of the LE structure in the heated zones, and the estimated/known material properties are given in Table I. This particular type of construction was required to meet the goals set forth for the validation program.

### III.2 Test Instrumentation

The model was heavily instrumented with type-T thermocouples, heat flux gages, and Resistance Temperature Detectors (RTD). A total of 76 sensors was used. The locations of several of the sensors are illustrated in Reference [1].

The development of the Cox TTMS began in the early 1980's, and has been used to support the design of ice protection systems for the F-14, OV-1, AH-64, B-1B, and SAAB 340 aircraft, among others. It performs two main functions: data acquisition and closed-loop control. It consists of data acquisition boards to measure analog input signals which are sent to a personal computer via data bus. These signals are converted to digital representation of physical measurements (temperature, heat flux, resistance) with a custom written software. The software then sends signals back to the power module in the TTMS to control the amount of power supplied to individual heater zones.

A user can request the TTMS to maintain a particular sensor at a desired temperature (e.g., to maintain the thermocouple temperature feedback on the metal skin constant). The TTMS will then control in a closed-loop and resolve the power density required for each heater to yield the desired temperature. Conversely, the user can simply set the power density to each heater independent of sensors temperature feedback (TTMS will disconnect the power in case the temperature exceeds a preset value).

Additional equipment was used to monitor the test. Video recorders were used throughout the tests to monitor surface runback and the ice growth. Still photographs were taken with 35 mm cameras to document ice shapes and residual ice following each run. An infrared camera setup was utilized to monitor the airfoil LE surface temperature from the IRT control room. A portion of the LE was coated with a thin black paint to increase the surface emissivity to near 0.96 (Bare metal normally has very low surface emissivity).

### III.3 Test Conditions

Anti-icing and de-icing runs were performed at two different airspeeds, several airfoil AOA's, and various meteorological conditions. These icing conditions are summarized in Table II. This paper is dedicated to the validation of the ANTICE program. Therefore, only anti-icing test runs will be discussed (evaporative and running-wet). For simplicity, and to focus on the physical analysis of the icing process with fewer experimental error uncertainties, only cases with zero degrees angle of attack will be considered in the comparison process. The large experimental database generated will be utilized to continue the validation process further.

## IV. Energy Balance Analysis and Discussions

Simulation of the icing process of aircraft surfaces is a challenging task. Several uncertainties exist as a result of the large number of variables involved in this problem. In order to understand the differences between the experimental data and the theoretical predictions, the energy balance terms will be illustrated. The various modes of heat transfer will be illustrated to study the contribution of each on the total power required for a running-wet system and an evaporative system.

The energy required to heat the aircraft skin to a specified temperature may be expressed in general terms as:

$$q = q_{conv} + q_{evap} + q_{sens} + q_{KE} \quad (1)$$

where the individual components are written as,

$$q_{conv} = h\,(T_s - T_{aw}) \quad (2)$$

$$q_{evap} = m_{evap}\,L_v \quad (3)$$

$$q_{sens} = m_{imp}\,C_{pw}\,(T_s - T4) \quad (4)$$

$$q_{KE} = m_{imp}\,V^2/(2\,g_c) \quad (5)$$

The runback heat of enthalpy was neglected in Eq. (1) for simplicity in illustrating the point. Besides, this term is negligible when the surface is controlled to a specified temperature in which case the runback is maintained at a constant temperature. The rate of water impingement is:

$$m_{imp} = \beta\,LWC\,V \quad (6)$$

The rate of water evaporation from the surface is a non-linear function of the surface temperature as described in Reference [6].

In order to identify the contribution of each term, two example cases will be considered: a cold condition at -22 ºF, and a warm condition at 20 ºF. These examples will be useful in the analysis of the ANTICE predictions when compared to the experimental data in the following section. The following parameters were selected as representative values:

h = 40 Btu/hr.ft$^2$.ºF
LWC = 0.39 g/m$^3$
β = 0.5
V = 200 mph

The heat required to keep the surface at specific range of temperatures was computed using Eq. (1). The total power density as well as each heat component were plotted in Figures 3 and 4 for the warm and cold conditions, respectively. The corresponding results expressed in terms of percentage of the total heat required are illustrated in Figures 5 and 6.

These plots show the strong dependence of total power required for evaporative anti-icing (normally in the range of 100 to 120 ºF) on the evaporation rate which is directly related to droplet impingement rates. On the other hand, to maintain the surface just above freezing, for example at 40 ºF, the total power required is highly dependent on the convective heat transfer coefficient and ambient temperature.

## V. Test Results and Comparisons

Several runs at different icing conditions (see Table I) were executed. Experimental results of most of the runs were summarized in Table III where the Run numbers and the corresponding TTMS file record number are shown. The measured skin temperatures and the heater power densities for each zone are displayed. The results and comparisons to the ANTICE predictions will be illustrated and discussed for each mode of anti-icing separately, running-wet and evaporative.

### V.1 Running-wet Anti-icing Cases:

In the running-wet conditions, the runback was maintained at temperatures a few degrees above freezing within the heated region. Beyond this region, the runback freezes along a distance that depends on several variables but mostly on temperature. Figures 10 and 11 show that effect. ANTICE normally predicts freezing within about 0.75" length for cold conditions and about 2" for warm and very wet (high LWC) conditions.

In the validation process, the measured power densities were then used as inputs to the ANTICE code. Comparisons between the predicted and measured skin temperatures will be the basis of validation in this paper. Few example cases will be illustrated as representative to the level of agreement between the theoretical and the experimental data. It is planned that all test runs will be summarized and made available on digital media, such as on a CD-ROM, along with ANTICE predictions for several runs.

In running-wet operations, the surface runback mass flow rate rapidly increases as it moves away

from the stagnation line within the direct impingement region. Since a small percentage is evaporating, the runback flow rate should reach a maximum just upstream of the impingement limits, and start to decrease slowly as it flows to downstream regions. To illustrate this phenomenon, consider the case of Run#22B (TTMS#71 as shown in Table III). This corresponds to icing condition 1 as illustrated in Table II.

Figure 12 illustrates the experimental as well as the ANTICE predicted skin temperature and surface mass flow rate distributions. The above discussion of surface mass flow rate is predicted by ANTICE. The surface temperatures are in excellent agreement with the measured values. This was not the case for the aft 2 heaters (D, E, F, and G) when the measured laminar heat transfer coefficients shown in Figures 8 and 9 were used. When the experimental film coefficient for the wet condition was plotted as shown in Figure 13, it was realized that the laminar flow is disturbed by the surface runback water (beads and rivulets) and transition to turbulent flow must have occurred just past about 1.25 inches. Therefore, the flow was manually tripped at those locations, and 2 new heat transfer coefficient distributions (one at 100mph and another at 200mph freestream velocities) were used thereafter in the remainder of the cases.

Additional running-wet cases illustrated in Figures 14 through 17 show a very good agreement with the experimental values. It should be realized that more studies must be conducted to predict the transition locations for different geometries at different airspeeds and surface runback physical structure and dimensions.

**V.2 Evaporative Anti-icing Cases:**

Evaporative anti-icing predictions were not as good as the running-wet cases. As discussed in Section IV, and as shown in Figures 5 and 6 for temperatures in excess of 100 ºF, approximately 70% of the total power required to achieve a fully evaporative operation (no runback beyond the heated zones) is the heat component required to evaporate surface water as given by Equation (3). This is a result of the high latent heat of vaporization of water.

This phenomenon is better understood through an example. Consider Run#22A (TTMS#70). Figure 18 illustrates the experiment film coefficient in a wet environment. The average wet film coefficient should superimpose the dry film or heat transfer coefficient beyond the direct impingement zone where the surface is dry. This occur near +/-2 inches from the hilite. Beyond those locations, the experimental film coefficient increases indicating that transition to turbulence has occurred. In a similar manner to the running-wet conditions, the boundary layer was manually tripped at those locations to predict the heat transfer coefficient distribution which was used for the remainder of the cases at the same freestream velocity.

Figure 19 shows the ANTICE code predictions for the skin temperature and the runback mass flow rate. The comparison is acceptable considering the large surface temperature variations within short distances as also observed in the IR camera thermographic data. Surface runback water disappear near and past the impingement limits confirming an evaporative system operation.

Figure 20 illustrates a typical behavior seen in many of the cases. In low airspeeds, 100mph here, a higher surface temperature is required to achieve full evaporation. The two main elements that promote evaporation are a higher mass transfer coefficient which is proportional to the heat transfer coefficient, and a high surface temperature. This was confirmed in all the experimental results and shown here in two examples: Figure 20 for the low airspeed of 100mph and Figure 21 for the high airspeed 200mph. Both cases were at the same ambient temperature (0 ºF). At 100mph, it was noticed that a surface temperature of about 150 ºF was required as opposed to 100 ºF in the case of 200mph.

Comparisons of the predicted temperatures to the experimental measurements in those two figures is subjective. In many cases, the code seems to predict the stagnation within about 10 ºF which is acceptable considering the measurement uncertainties and the number of environmental variables involved. However, the skin temperature at zones B&C, adjacent to the hilite heater, are always underpredicted by ANTICE (by 25 ºF or more). This may be associated with two reasons: (1) many of the conditions were near the edge of the spray bar calibration envelope which could result in smaller LWC than actually predicted by the calibration standard; (2) the predicted rate of mass evaporation is always assumed to get 100% of the latent energy from the skin and absolutely none from the heated boundary layer. A closer look should be given to all variables throughout the icing simulation (experimental and computational).

## VI. Concluding Remarks

An experimental program was generated by the Icing Technology Branch at NASA Lewis Research Center to validate two ice protection simulation codes: LEWICE/Thermal and ANTICE. This paper was dedicated to the validation of ANTICE, a steady state hot gas and electrothermal anti-icing simulations. An electrothermal ice protection system was designed and constructed integral to a 36 inch chord NACA0012 airfoil. The model was fully instrumented with thermocouples, RTD's, and heat flux gages. Tests were successfully conducted at several icing environmental conditions in the NASA Lewis Icing Research Tunnel (IRT). Experimental results of running-wet and evaporative cases were compared to the ANTICE computer code predictions.

The dry heat transfer coefficients predicted by LEWICE, when forced to stay laminar, were in general good agreement with the measured values. This distribution was slightly higher in the experimental cases than in the theoretical predictions. The difference can be attributed to the fact that the IRT is not considered as a low turbulence aerodynamic tunnel and its main purpose is to simulate icing environments. In the validation process, the experimental values were used in the laminar region to isolate the effect of that variable on the ANTICE temperature predictions.

The computer code predictions for running-wet anti-icing conditions were very close to the experimental measurements. However, this agreement near the aft zone heaters was realized when the laminar boundary layer (BL) was forced to trip at these locations as depicted in the experimental results of the film coefficient distribution in wet conditions.

The ANTICE code predictions of the skin temperatures in the evaporative cases were acceptable near stagnation, but marginal elsewhere especially at zones B&C. This is due to the large effects of the evaporative cooling which is directly attributed to the high latent heat of vaporization of water. An accurate measurement of LWC and verification of the collection efficiency distribution are required to evaluate any deficiencies in the standard evaporative terms used in most icing simulation codes. Nevertheless, ANTICE predicted no runback existed past the heated zones in most cases. Interestingly, evaporative anti-icing is more dependent on the power requirements and not the standard surface temperature of 120 ºF normally assumed. In low velocity conditions (low h), the surface reached over 150 ºF to achieve fully evaporative conditions.

One should not expect to always correctly predict the skin temperature at the aft heater zones because the difference between having little or no runback at those regions can be as high as 100 ºF. Heaters at those regions must be designed such that they protect against the majority of icing condition requirements without exceeding the material temperature limits in the dry conditions at the low aircraft airspeed of its operational envelope.

Future recommended studies:

1. Develop a model that will predict the transition location and the heat transfer coefficients for different conditions. The BL seems laminar for a relatively wide portion of the leading edge (LE) as opposed to what LEWICE normally predicts. Experimental results show that the BL is definitely affected by surface water runback (beads and rivulets). The transition location is moved further downstream in evaporative anti-icing cases but the transition to turbulent is milder.

2. Revisit the evaporative cooling law as applied to aircraft icing. Studies of the basic physics must be conducted to isolate the various modes of heat transfer, especially the evaporative mass and energy transfer from the surface. These studies must also verify the cloud LWC and the water droplet collection efficiency at the LE of the model. The effect of heating the surface and evaporation on the BL must also be considered.

3. Carefully analyze all the records in the relatively large experimental database, and conduct a thorough validation process with sensitivity analysis. This, for example, includes verification of thermocouple readings with thermographic data from the Infrared camera.

## Acknowledgments

This work was sponsored by the Icing Technology Branch at the *NASA Lewis Research Center*, Cleveland, Ohio.

## References

[1]Miller, D.R., Bond, T.H., Sheldon, D.W., Wright, W.B., Langhals, T., Al-Khalil, K.M., Broughton, H., "Validation of NASA Thermal Ice Protection Computer Codes: Part 1 - Program Overview", AIAA Paper 97-0049, Jan 1997.

[2]Wright, W.B., Al-Khalil, K.M., Miller, D.R., "Validation of NASA Thermal Ice Protection Computer Codes: Part 2 - The Validation of LEWICE/Thermal", AIAA Paper 97-0050, Jan 1997.

[3]Al-Khalil, K.M., Keith, T.G., and De Witt, K.J., "Further Development of an Anti-Icing Runback Model," AIAA Paper 91-0266, Jan. 1991.

[4]Al-Khalil, K.M., Keith, T.G., and De Witt, K.J., "Development of an Improved Model for Runback Water on Aircraft Surfaces," AIAA Paper 92-0042, Jan. 1992.

[5]Wright, W.B., "Users Manual for the Improved NASA Lewis Ice Accretion Code LEWICE 1.6", NASA CR-198355, June 1995.

[6]Al-Khalil, K.M., Keith, T.G., De Witt, K.J., Nathman, J.K., Dietrich, D.A., "Thermal Analysis of Engine Inlet Anti-Icing Systems," *Journal of Propulsion and Power*, Vol. 6, No. 5, Sept-Oct, 1990, pp. 628-634.

**Table I: Leading Edge Material Properties**

| ITEM | MATERIAL | K (Btu/hr.ft.ºF) | ρ (lbm/ft$^3$) | $C_p$ (Btu/lbm.ºF) |
|---|---|---|---|---|
| 1 | Heating Element (alloy 90) | 23.7 | 556 | 0.092 |
| 2 | Erosion Shield (SS 301 HH) | 9.4 | 501 | 0.12 |
| 3 | Elastomer (Cox 4300) | 0.148 | 86.4 | 0.30 +/-0.03 |
| 4 | Fiberglass/Epoxy Composite | 0.17 | 112 | 0.375 |
| 5 | Silicone Foam Insulation | 0.07 | 40.5 | 0.27 +/-0.03 |

**Table II: Icing Conditions Tested at the NASA LeRC IRT**

| Icing Condition | $T_{tot}$ (ºF) | V (mph) | LWC (g/m$^3$) | MVD (:m) | AOA (degrees) |
|---|---|---|---|---|---|
| 1 | 20 | 100 | .78 | 20 | 0 |
| 2 | 20 | 100 | 1.1 | 20 | 0 |
| 3 | 20 | 200 | .39 | 20 | 0 |
| 4 | 0 | 100 | .78 | 20 | 0 |
| 5 | 0 | 100 | 1.1 | 20 | 0 |
| 6 | 0 | 200 | .39 | 20 | 0 |
| 7 | 20 | 200 | .55 | 20 | 0 |
| 8 | 0 | 200 | .55 | 20 | 0 |
| 9 | 20 | 100 | .78 | 20 | -2 |
| 10 | 20 | 100 | .78 | 20 | -4 |
| 11 | 20 | 100 | .90 | 40 | 0 |
| 12 | -22 | 200 | .39 | 20 | 0 |
| 13 | 15 | 100 | 2.0 | 20 | 0 |
| 14 | 0 | 100 | .78 | 20 | -2 |
| 15 | 0 | 100 | .78 | 20 | -4 |

**Table III: Summary of Measured Skin Temperatures and Heater Power Densities (Evaporative and Running-wet Anti-Icing Modes)**

| Icing Cond-ition | Run # (TTMS#) | Anti-Icing Mode | Zone A | | Zone B | | Zone C | | Zone D | | Zone E | | Zone F | | Zone G | |
|---|---|---|---|---|---|---|---|---|---|---|---|---|---|---|---|---|
| | | | $T_s$ | q | $T_s$ | q | $T_s$ | q | $T_s$ | q | $T_s$ | q | $T_s$ | q | $T_s$ | q |
| 1 | 22 | Evap | 117 | 30 | 147 | 21 | 150 | 12 | 160 | 6.6 | 162 | 4.5 | 157 | 6.4 | 156 | 6.6 |
| | (70,71) | Wet | 38 | 3.1 | 40 | 2.6 | 40 | 1.9 | 40 | 1.9 | 39 | 2.2 | 40 | 1.7 | 38 | 1.5 |
| 2 | 48 | Evap | 116 | 30 | 158 | 27 | 163 | 19 | 169 | 8.2 | 172 | 4.3 | 165 | 7.6 | 164 | 8.8 |
| | (75,76) | Wet | 37 | 3.2 | 39 | 2.6 | 40 | 2.3 | 39 | 2.0 | 39 | 2.3 | 38 | 1.7 | 39 | 1.7 |
| 3 | 53 | Evap | 92 | 24 | 97 | 17 | 100 | 12 | 103 | 6.7 | 106 | 3.0 | 100 | 6.2 | 101 | 5.3 |
| | (80,81) | Wet | 36 | 4.2 | 38 | 3.4 | 38 | 3.4 | 37 | 3.5 | 36 | 3.8 | 35 | 2.6 | 35 | 2.4 |
| 4 | 35 | Evap | 112 | 30 | 144 | 22 | 151 | 15 | 154 | 7.6 | 157 | 4.3 | 150 | 7.8 | 149 | 8.2 |
| | (63,64) | Wet | 36 | 5.8 | 38 | 4.5 | 39 | 3.8 | 38 | 3.8 | 38 | 4.0 | 36 | 3.1 | 36 | 2.9 |
| 5 | 58 | Evap | 112 | 30 | 133 | 25 | 155 | 22 | 163 | 11 | 174 | 8.0 | 153 | 11 | 159 | 12 |
| | (114,115) | Wet | 38 | 6.3 | 41 | 4.8 | 40 | 3.6 | 42 | 4.2 | 40 | 4.2 | 41 | 3.4 | 40 | 3.2 |
| 6 | 63 | Evap | 92 | 27 | 98 | 19 | 102 | 14 | 102 | 9.3 | 105 | 5.4 | 93 | 11 | 89 | 9.4 |
| | (116,117) | Wet | 47 | 10 | 48 | 8.0 | 49 | 7.2 | 47 | 9.1 | 47 | 9.1 | 46 | 6.7 | 46 | 6.3 |
| 7 | 65 | Evap | 102 | 30 | 128 | 28 | 135 | 22 | 145 | 10 | 151 | 3.1 | 142 | 5.6 | 136 | 9.3 |
| | (101,102) | Wet | 38 | 4.9 | 39 | 3.8 | 39 | 3.6 | 38 | 4.0 | 38 | 4.4 | 37 | 3.1 | 37 | 2.9 |
| 8 | 67 | Evap | 91 | 28 | 97 | 21 | 99 | 17 | 100 | 14 | 101 | 12 | 94 | 13 | 95 | 12 |
| | (104,105) | Wet | 42 | 9.8 | 43 | 7.0 | 45 | 6.4 | 43 | 7.7 | 42 | 8.3 | 38 | 5.4 | 42 | 5.6 |
| 9 | 69 | Evap | 117 | 30 | 164 | 18 | 163 | 19 | 170 | 6.1 | 172 | 3.8 | 164 | 8.7 | 169 | 4.9 |
| | (92,93) | Wet | 38 | 3.1 | 40 | 2.6 | 40 | 1.9 | 40 | 1.9 | 40 | 1.9 | 39 | 1.7 | 39 | 1.7 |
| 10 | 71 | Evap | 117 | 30 | 154 | 13 | 151 | 24 | 154 | 6.6 | 160 | 5.4 | 147 | 11 | 135 | 4.5 |
| | (95,96) | Wet | 39 | 3.5 | 41 | 2.6 | 39 | 1.9 | 41 | 2.5 | 40 | 2.0 | 40 | 2.0 | 40 | 2.0 |
| 11 | 73 | Evap | 116 | 30 | 141 | 27 | 150 | 22 | 157 | 9.2 | 168 | 5.3 | 157 | 7.7 | 154 | 8.4 |
| | (98,99) | Wet | 40 | 4.0 | 41 | 2.8 | 42 | 2.6 | 42 | 2.5 | 40 | 2.5 | 41 | 2.0 | 41 | 2.0 |
| 12 | 75 | Evap | 91 | 30 | 122 | 28 | 125 | 23 | 132 | 11 | 132 | 11 | 116 | 15 | 102 | 15 |
| | (124,125) | Wet | 45 | 15 | 47 | 10 | 47 | 9.0 | 46 | 12 | 45 | 13 | 44 | 9.4 | 45 | 8.9 |
| 13 | 87 | Evap | -- | -- | -- | -- | -- | -- | -- | -- | -- | -- | -- | -- | -- | -- |
| | (110) | Wet | 37 | 4.6 | 39 | 3.5 | 39 | 2.6 | 39 | 2.5 | 39 | 2.5 | 39 | 2.2 | 38 | 2.0 |
| 14 | 89 | Evap | 114 | 30 | 175 | 22 | 168 | 24 | 190 | 8.9 | 192 | 5.0 | 167 | 12 | 168 | 6.4 |
| | (119) | Wet | -- | -- | -- | -- | -- | -- | -- | -- | -- | -- | -- | -- | -- | -- |
| 15 | 91 | Evap | 113 | 30 | 160 | 16 | 151 | 28 | 161 | 11 | 166 | 5.5 | 153 | 14 | 160 | 7.8 |
| | (122,123) | Wet | 40 | 6.3 | 43 | 4.5 | 42 | 3.9 | 43 | 4.7 | 43 | 3.4 | 43 | 3.9 | 43 | 3.7 |

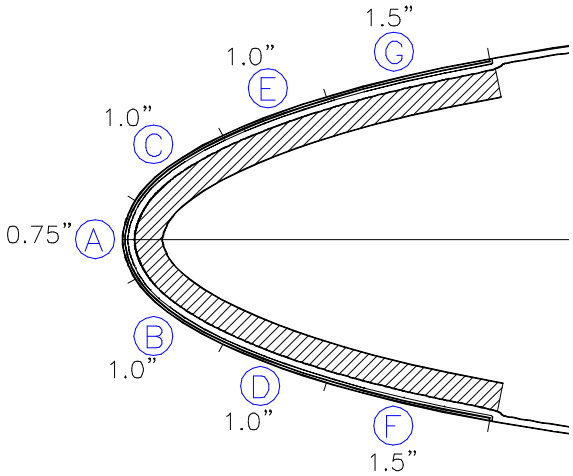


*Figure 1: Cross-section of the airfoil leading edge and heated zones*

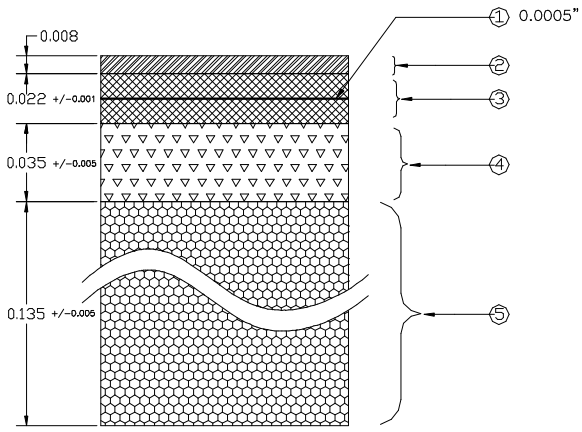


*Figure 2: Leading edge material composition (see Table I)*

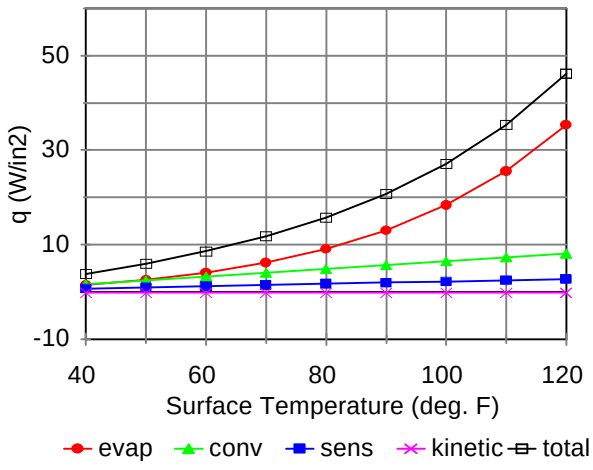


*Figure 3: Energy balance terms at $T_{tot}$ = 20 ºF*

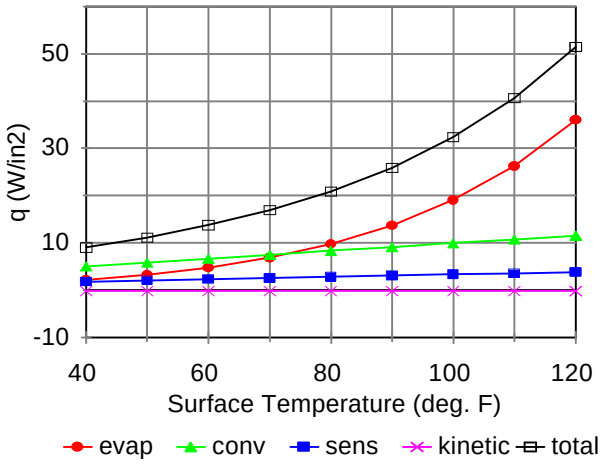


*Figure 4: Energy balance terms at $T_{tot}$ = -22 ºF*

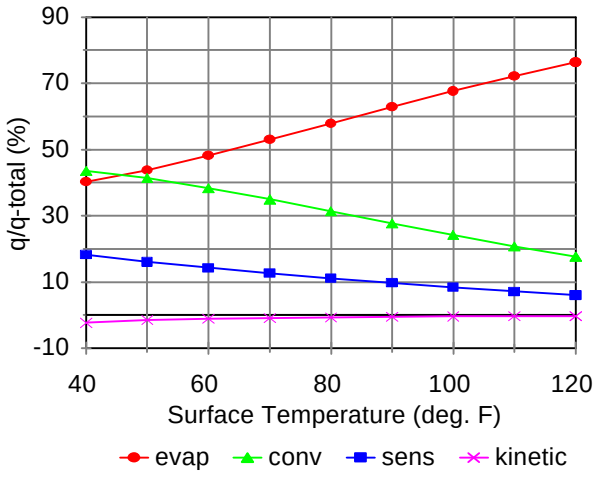


*Figure 5: Energy balance terms at $T_{tot}$ = 20 ºF in percentage of total heat required*

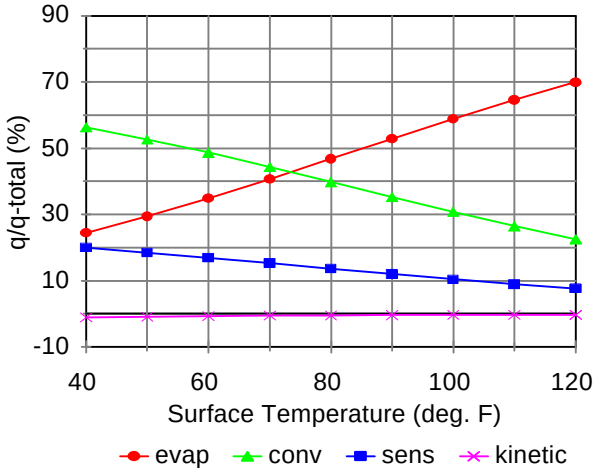


*Figure 6: Energy balance terms at $T_{tot}$ = -22 ºF in percentage of total heat required*

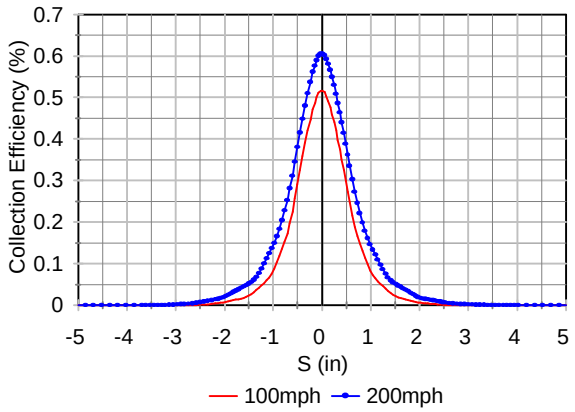


*Figure 7: Predicted collection efficiencies*

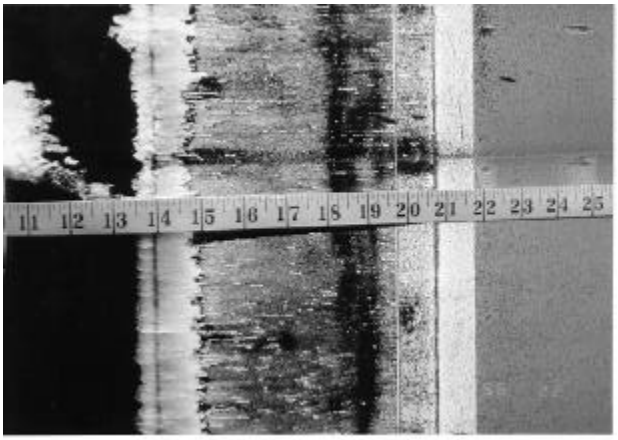

*Figure 10: Typical runback in a running-wet anti-icing case at cold ambient temperatures*

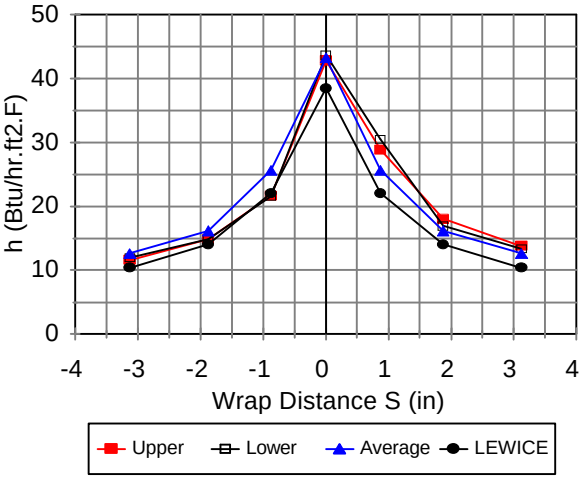


*Figure 8: Experimental and LEWICE predictions of h at V=100mph (Run#22, TTMS#51)*

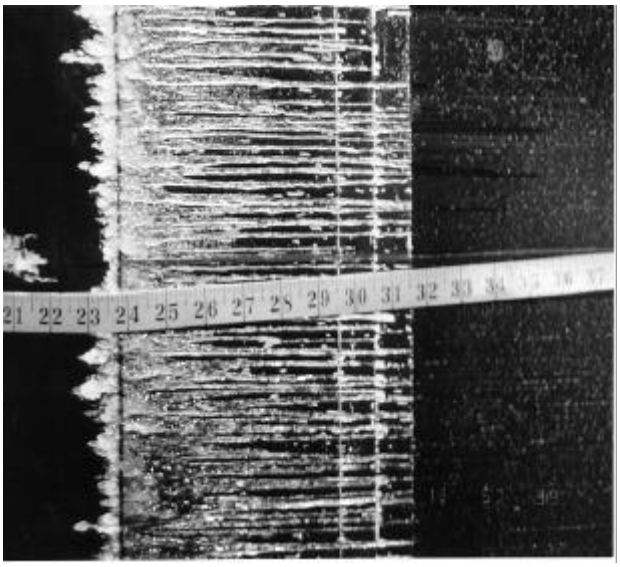

*Figure 11: Typical runback in a running-wet anti-icing case at warm ambient temperatures*

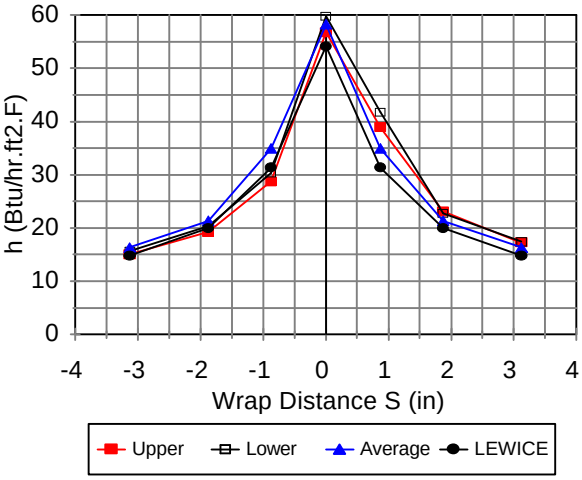


*Figure 9: Experimental and LEWICE predictions of h at V=200mph (Run#13, TTMS#42)*

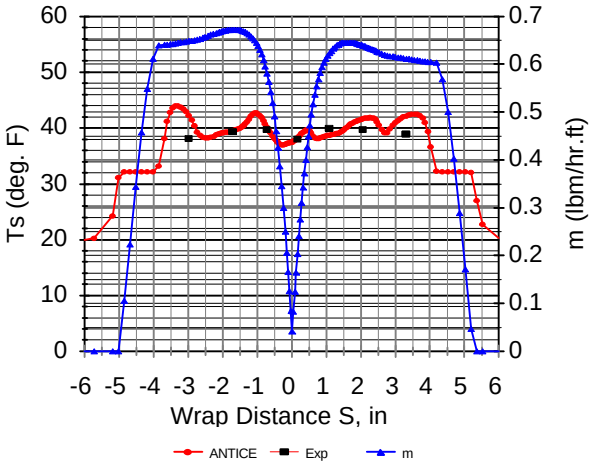


*Figure 12: Experimental and ANTICE predictions for Run#22B (TTMS#71, running-wet)*

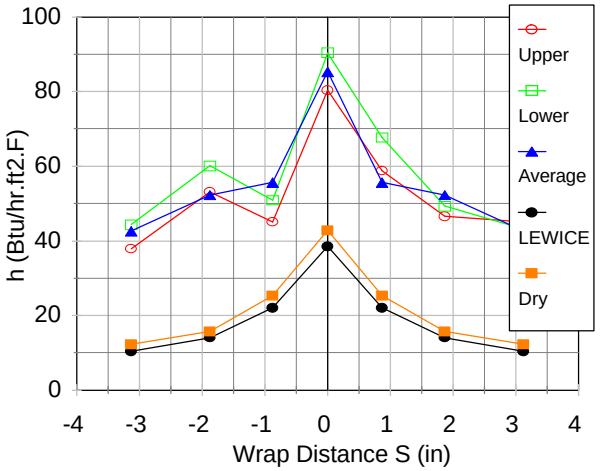


*Figure 13: Experimental film coefficient for Run#22B (TTMS#71, running-wet)*

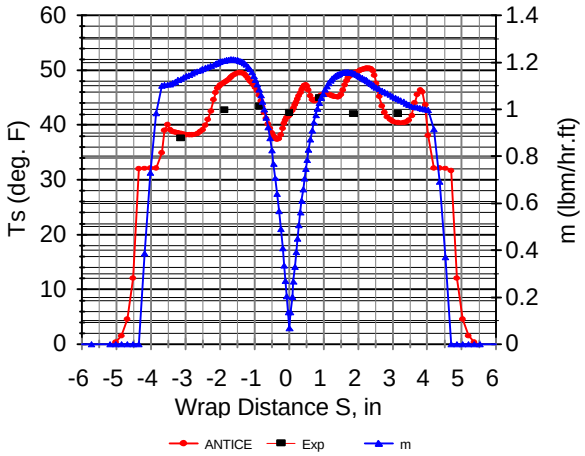


*Figure 16: Experimental and ANTICE predictions for Run#67B (TTMS#105, running-wet)*

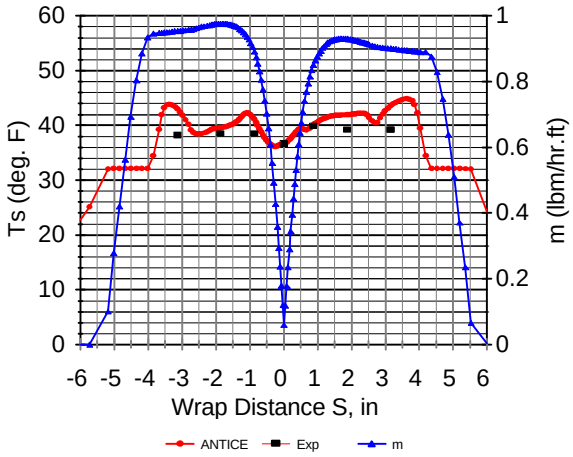


*Figure 14: Experimental and ANTICE predictions for Run#48B (TTMS#76, running-wet)*

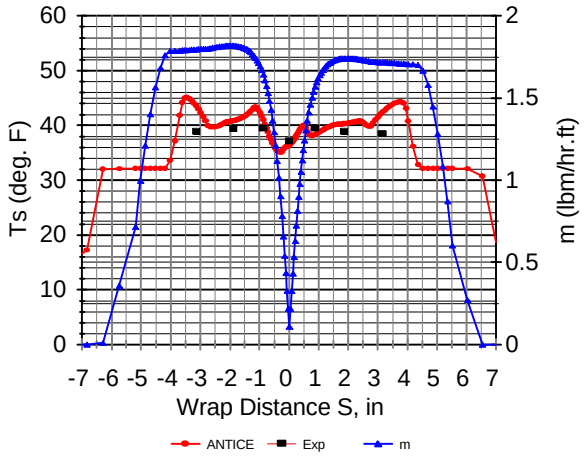


*Figure 17: Experimental and ANTICE predictions for Run#87 (TTMS#110, running-wet)*

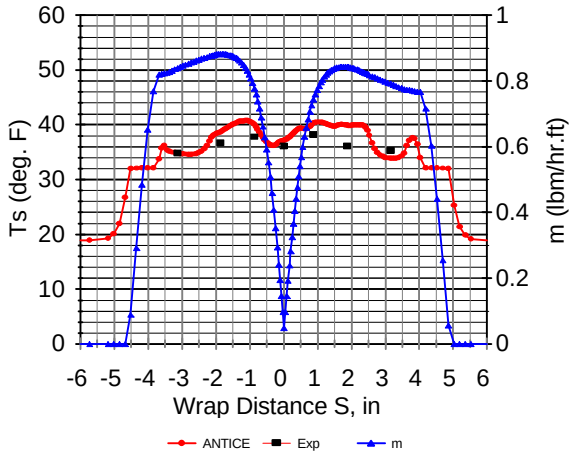


*Figure 15: Experimental and ANTICE predictions for Run#53B (TTMS#81, running-wet)*

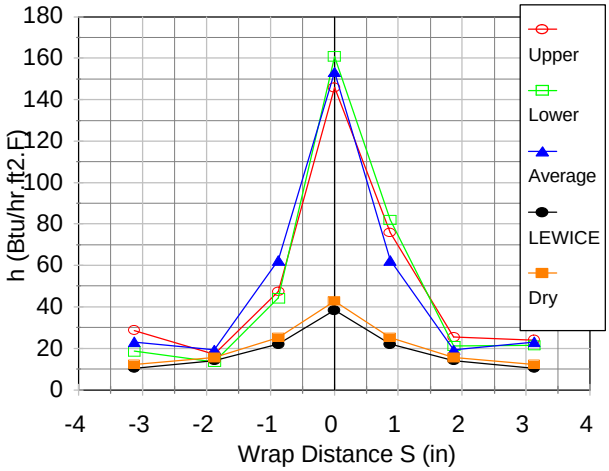


*Figure 18: Experimental film coefficient for Run#22A (TTMS#70, evaporative)*

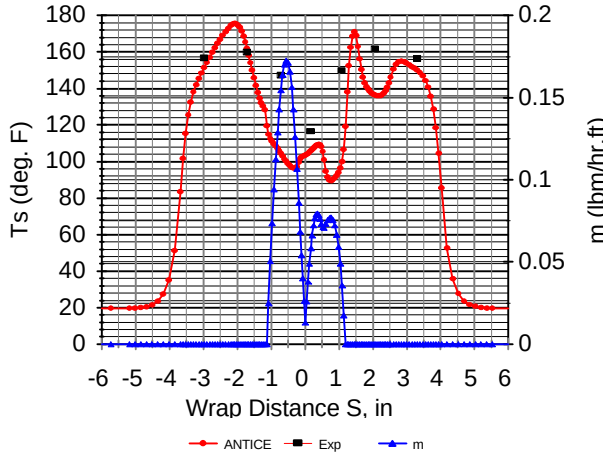


*Figure 19: Experimental and ANTICE predictions for Run#22A (TTMS#70, evaporative)*

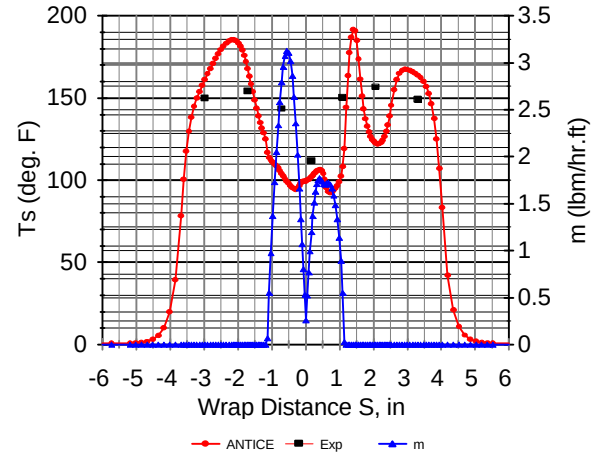


*Figure 20: Experimental and ANTICE predictions for Run#35A (TTMS#63, evaporative)*

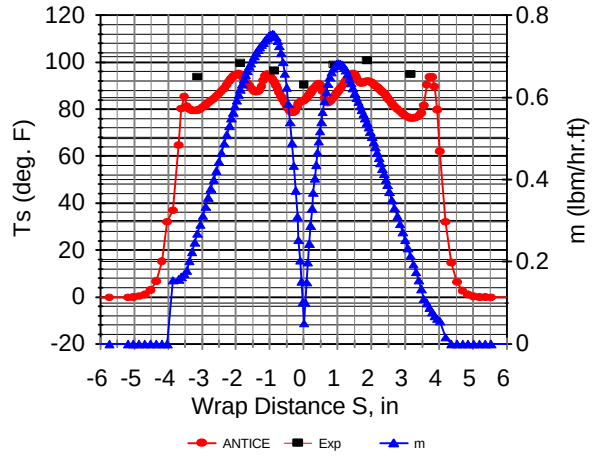


*Figure 21: Experimental and ANTICE predictions for Run#67A (TTMS#104, evaporative)*